Research Repository UCD

Provided by the author(s) and University College Dublin Library in accordance with publisher policies. Please cite the published version when available.

Title	Fundamental diffraction limitations in a paraxial 4-f imaging system with coherent and incoherent illumination
Authors(s)	Kelly, Damien P.; Sheridan, John T.; Rhodes, William T.
Publication date	2007-07-01
Publication information	Journal of the Optical Society of America A, 24 (7): 1911-1919
Publisher	Optical Society of America
Link to online version	http://dx.doi.org/10.1364/JOSAA.24.001911
Item record/more information	http://hdl.handle.net/10197/3374
Publisher's statement	This paper was published in Journal of the Optical Society of America A and is made available as an electronic reprint with the permission of OSA. The paper can be found at the following URL on the OSA website: http://www.opticsinfobase.org/abstract.cfm?URI=josaa-24-7-1911. Systematic or multiple reproduction or distribution to multiple locations via electronic or other means is prohibited and is subject to penalties under law.
Publisher's version (DOI)	10.1364/JOSAA.24.001911

Downloaded 2022-08-23T12:21:46Z

The UCD community has made this article openly available. Please share how this access benefits you. Your story matters! (@ucd_oa)

Fundamental diffraction limitations in a paraxial 4-*f* imaging system with coherent and incoherent illumination

Damien P. Kelly,[1] John T. Sheridan,[2,*] and William T. Rhodes[3]

[1]*Institut für Photonik und Zentrum für Mikro- und Nanostrukturen, Technische Universität Wien, A-1040 Wien, Austria*

[2]*School of Electrical, Electronic and Mechanical Engineering, College of Engineering, Mathematical and Physical Sciences, University College Dublin, Belfield, Dublin 4, Ireland*

[3]*Imaging Technology Center, Florida Atlantic University, 777 Glades Road, Building 43, Room 486, Boca Raton, Florida 33431, USA*

**Corresponding author: john.sheridan@ucd.ie*

Received October 20, 2006; revised February 12, 2007; accepted February 14, 2007; posted March 2, 2007 (Doc. ID 76181); published June 13, 2007

In the usual model of an imaging system, only the effects of the aperture stop are considered in determining diffraction-limited system performance. In fact, diffraction at other stops—those associated with different lens elements, for example—can also affect system performance and cause the imaging to be space variant, even in the absence of vignetting in the conventional ray optics sense. For the 4-*f* imaging system investigated in this paper, the severity of the space variance depends on the relative sizes of the two lens stops and the aperture stops. If the diameters of the lenses are equal, the aperture of the first lens has a greater effect on system performance than does that of the second. © 2007 Optical Society of America

OCIS codes: 070.0070, 070.6020, 110.0110, 110.0220, 110.2990.

1. INTRODUCTION

The analysis of optical imaging systems can be approached in many ways [1–8]. For example, with a simple ray-based analysis, system magnification, entrance and exit pupil locations, and vignetting conditions can easily be determined [3,4]. The effects of diffraction are calculated using wave optics tools [1,3]. Often the wave optics description is simplified [3]. For example, even though an imaging system may consist of several optical elements, each with its own aperture, these elements are often lumped together in a single "black box," and only a projected image of the system's limiting aperture, i.e., the exit or the entrance pupil, is used to describe the effects of diffraction [3]. In the paraxial regime, this simplified analysis results in a linear, shift-invariant (LSI) description of the imaging operation for spatially incoherent objects, and a simple convolution operation describes the object–image relationship. In this paper we examine the fundamental limits of this black box approximation in detail for the special case of the 4-*f* imaging system by examining the effect of diffraction from the lens apertures as well as from the limiting aperture. Our analysis shows that these diffraction effects destroy the space invariance of the imaging operation, to an extent determined by the relative sizes of the various apertures.

The basic notion is illustrated with the help of Fig. 1. A point source (PS), located in the front focal plane of lens L_1, emits a diverging spherical wave that is incident upon lens L_1. If the lens is infinite in diameter, the spherical wave will be transformed into an ideal plane wave traveling at some angle to the optical axis, and diffraction effects are first introduced by the limiting aperture in the Fourier plane (FP in the figure). If L_1 is not infinite in extent, however, the wave leaving L_1 is subject to the effects of diffraction by the lens aperture itself. The consequences of this diffraction depend on the location of the point source, and the imaging operation is thus space variant and must be described not by a convolution integral but rather by a more general superposition integral, a superposition model (SPM) resulting. We explicitly define these two models, LSI and SPM, in Section 2.

In Section 3 we investigate differences between the LSI and the SPM models by examining how the plane-wave (L_1 infinite) and the plane wave segment (L_1 finite) distributions differ from each other in the Fourier plane. By examining deviations between these two cases, we establish a relationship between the locations of the magnitude and phase deviation extrema and the parameters of the optical system, i.e., the diameter and focal length of L_1 and the wavelength of the illuminating light. We then proceed to compare the point-spread functions (PSFs) of the LSI and SPM models for point sources located both on and off axis. A modified version of the optical transfer function (OTF) for the SPM model is derived and discussed. We compare the LSI and SPM predictions for the image plane distribution when a straight edge is imaged for both coherent and incoherent illumination. Finally, in this section we examine the effect of the finite extent of the second lens, L_2, in the 4-*f* system. We show that once L_2 becomes larger than L_1, L_2 can be considered to be effectively infinite.

In our analysis we assume that the imaging systems

 © 2007 Optical Society of America

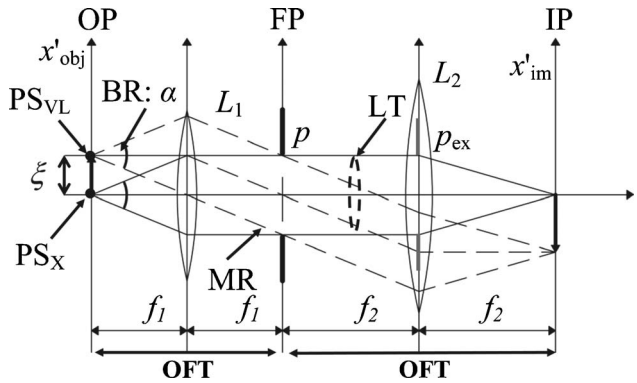

Fig. 1. 4-*f* imaging system. OP, object plane; FP, Fourier (aperture) plane; IP, image plane; MR, marginal ray; LT, light tube; BR: α, bundle of rays (defined by cone angle α); OFT, optical transfer function.

are diffraction limited and that a paraxial scalar model is sufficiently accurate. In many practical cases this is not true; even expensive lenses suffer from aberrations [1,7], and in high numerical aperture and confocal scanning microscopy [8,9] a scalar model is not capable of accurately describing details of the imaging operation. Nevertheless, the relative simplicity of a scalar model allows significant insight into resolution limits and image formation [6] and can be used to determine, with reasonable accuracy, the limits of the commonly used black box model outlined by Goodman [3] and others [1,4–9].

In Section 2 we present the linear equations that describe an image-forming system, identifying two cases: (i) a linear system that is not shift invariant and must be described using a superposition integral and (ii) a simpler LSI model that can be described using a convolution integral. It is necessary at this point to also briefly discuss vignetting in a 4-*f* imaging system using a ray optics approach. In Section 3 we compare the LSI and SPM models by examining the PSF, the OTF, and the imaging of a semi-infinite straight edge. We then show the input lens, L_1, has a more significant effect on the system performance than L_2 once the diameter of L_2 is greater than or equal to L_1. Finally, in Section 4 we present a brief conclusion of the results of the paper. In what follows, for both clarity and brevity, we restrict ourselves to presenting a 2-D analysis (x and z).

2. LINEAR SYSTEM MODEL OF AN IMAGING SYSTEM

A linear optical imaging system operating on input object field $U_{obj}(x'_{obj})$ can be described by the superposition integral [3]

$$U_{im}(x'_{im}) = \int_{-\infty}^{\infty} h(x'_{im};\varsigma)U_g(\varsigma)\mathrm{d}\varsigma, \tag{1}$$

where $h(x'_{im};\varsigma)$ is the PSF of the optical system and where U_g, the geometrical optics image, is given by

$$U_g(\varsigma) = \sqrt{\frac{1}{M}}U_{obj}\left(\frac{\varsigma}{M}\right), \tag{2}$$

M representing the system magnification. Equations (1) and (2) describe a linear but not necessarily shift-invariant imaging system. If the system can be considered to be shift invariant, the superposition integral reduces to a convolution:

$$U_{im}(x'_{im}) = \int_{-\infty}^{\infty} h(x'_{im} - \psi)U_g(\psi)\mathrm{d}\psi, \tag{3}$$

where the PSF, $h(x_{im})$, is now given by [3]

$$h(x'_{im}) = \frac{A}{\sqrt{\lambda d_{ex}}}\int_{-\infty}^{\infty} p_{ex}(x)\exp\left(\frac{-j\pi x x'_{im}}{\lambda d_{ex}}\right)\mathrm{d}x. \tag{4}$$

In this expression A is a constant, d_{ex} is the distance from the exit pupil to the image plane, and $p_{ex}(x)$ is the exit pupil function. Note that $h(x_{im})$ is a scaled Fourier transform of the exit pupil function. The exit pupil is an image of the system's limiting aperture, given by pupil function

$$p(x) = \begin{cases} 1, & |x| \le a \\ 0, & \text{otherwise} \end{cases}, \tag{5}$$

where a is the radius of the aperture. When $d_{ex}=f_2$, both the exit pupil and the physical limiting aperture are described by Eq. (5).

Because of vignetting, only a central region in the object plane can be imaged without the operation becoming space variant. Vignetting can be introduced by the finite aperture of the input lens L_1 (see Fig. 1). We begin by examining vignetting in a 4-*f* system using a ray-based analysis. In Fig. 2 we see that for point source PS_{VL}, the marginal ray of light, delimiting the upper boundary of the bundle of rays defined by the cone angle α, just grazes the aperture of L_1. Nevertheless, the limiting aperture in the Fourier plane is still fully illuminated by a light tube of width $2a$, and all of the rays in the bundle are mapped to a corresponding bundle in the image plane (see Fig. 1).

PS_Q in Fig. 2, lying farther off axis than PS_{VL}, will produce a bundle of rays with a cone angle α. However, in this instance the aperture of the lens L_1 will ensure that not all of the rays are mapped from the object plane to the image plane, with a corresponding reduction in the amount of light reaching the image plane. Thus PS_{VL}

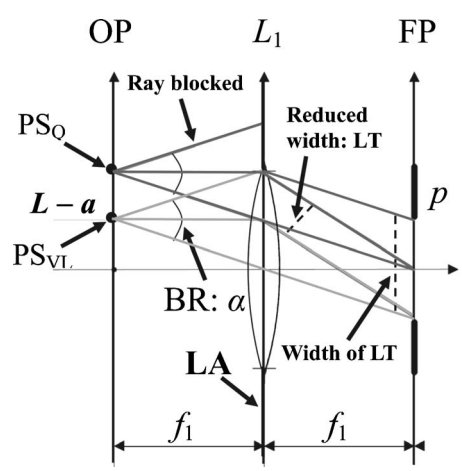

Fig. 2. Example of vignetting in the first OFT module of a 4-*f* imaging system for off-axis PS_{VL} and even farther off-axis point PS_Q. OP, object plane; FP, Fourier (aperture) plane; LA, lens aperture; LT, light tube; BR:α, bundle of rays (defined by cone angle α).

marks the onset of vignetting in the geometrical optics regime, and we use the subscript VL to refer to this point as the vignetting limit. We note that PS_{VL} lies a distance $L-a$ off axis.

Note that for PS_Q in Fig. 2 the aperture delimiting L_1 eliminates part of the light tube associated with PS_Q, and the aperture in the Fourier plane is thus no longer fully illuminated. From Eqs. (3) and (4) we recall that the PSF is given by a scaled Fourier transform of p. However, with vignetting, the region of the Fourier plane aperture that is no longer illuminated cannot contribute to the distribution in the image plane. This condition effectively reduces the size of that aperture and changes its shape, causing the integration limits in Eq. (3) to change and the corresponding PSF to broaden [5]. Thus for points that are located farther off axis than the vignetting limit the form of the PSF changes as a function of object point position. In this case the LSI properties do not hold, and the convolution relationship given in Eq. (3) no longer describes the imaging system behavior. Later in Section 3 we include these vignetting effects due to L_1 in our LSI model in order to compare deviations that are due to diffraction.

3. FINITE-LENS APERTURE EFFECTS IN A 4-*f* IMAGING SYSTEM

In the conventional analysis of 4-*f* imaging systems it is generally assumed that the effect of diffraction from the lens apertures is negligible and that the LSI model of Section 2 provides an adequate description of system behavior [7]. In this section we examine this assumption in detail and quantify the effects of diffraction by the input lens aperture. We incorporate these effects by using the Fresnel transform to describe the evolution of the wave segment that propagates from the lens plane to the Fourier plane. This approach is similar both conceptually and mathematically to that considered in Refs. [10,11]. For most of this section we assume that the diameter of L_2 is infinite, postponing a discussion of its effect until Subsection 3.E.

This section is structured as follows. In Subsection 3.A we examine the magnitude and phase deviations between the LSI and the SPM predictions of the field in the Fourier plane. In Subsection 3.B we compare the corresponding distributions in the image plane using a root-mean-square error (RMSE) metric denoted Ω. The variation of the Ω as a function of λ is then examined, and we show that as λ decreases, Ω decreases. In Subsection 3.C we examine the deviations between the LSI and the SPM predictions using the OTF. In Subsection 3.D we compare the LSI and SPM models for the case of the imaging of a semi-infinite straight edge. Finally, in Subsection 3.E we examine the effect of diffraction from the edge (aperture) of the second lens, L_2.

A. Deviations in the Field Distribution at the Fourier Plane

First, we describe LSI imaging, i.e., when the diameter of L_1 is sufficiently large that it can be considered infinite. A spherical wavefront incident on L_1 due to PS_O located a distance ξ' off axis in the object plane can be described as

$$U_{L_1}(x_L',\xi') = \exp\left[\frac{j\pi}{\lambda f_1}(x_L'-\xi')^2\right]. \tag{6}$$

After passing through a thin lens of infinite extent it assumes the form of a plane wave,

$$U_{\mathrm{pw}}(x,\xi) = \exp(-j2\pi Kx\xi), \tag{7}$$

where $K=\pi L^2/\lambda f_1$, $\xi=\xi'/L$, and $x=x'/L$ (normalized with respect to L, the radius of lens L_1). We neglect all constant phase terms. $U_{\mathrm{pw}}(x,\xi)$ is a plane wave that has a linear phase proportional to ξ but is not a function of z. It is this wave field that is incident on the aperture in the Fourier plane.

We now examine the SPM predictions by letting L_1 have finite extent. Using the Fresnel transform to model the propagation of light from the lens, we can write the distribution incident on the aperture in the Fourier plane as

$$U_{\mathrm{ap}}(x_{\mathrm{ap}}') = \frac{1}{\sqrt{j\lambda f_1}}\int_{-L}^{+L} U_{L_1}(x_L',\xi')\exp\left[\frac{j\pi}{\lambda f_1}(x_L'-x_{\mathrm{ap}}')^2\right]\mathrm{d}x_L'. \tag{8}$$

Rewriting in normalized coordinates and dropping any constant phase terms give

$$\begin{aligned} U_{\mathrm{ap}}(x_{\mathrm{ap}}) &= \sqrt{\frac{K}{j\pi}}\int_{-1}^{1}\exp\{jK[X^2+x_{\mathrm{ap}}^2-2X(x_{\mathrm{ap}}+\xi)]\}\mathrm{d}X \\ &= \frac{1}{2}[\exp(-j2\pi Kx_{\mathrm{ap}}\xi)]\{\mathrm{erfi}[\sqrt{jK}(x_{\mathrm{ap}}+\xi-1)] \\ &\quad -\mathrm{erfi}[\sqrt{jK}(x_{\mathrm{ap}}+\xi+1)]\}, \end{aligned} \tag{9}$$

where $X=x_L/L$, $x_{\mathrm{ap}}=x_{\mathrm{ap}}'/L$, $\xi=\xi'/L$, and erfi(−) is the imaginary error function [12–14].

In Fig. 3 we plot the magnitude of $U_{\mathrm{ap}}(x_{\mathrm{ap}})$ for $K=15.7$ and $\xi=0.5$. We note that this value of K corresponds to a system where $L=f_1=10$ cm and $\lambda=2$ cm, an unusually large value for the wavelength. For the remainder of this section, values of K of the order $K\sim 15.7$ will be used so that deviations between the LSI and the SPM models are emphasized. Returning to Fig. 3, we can see that the magnitude distribution is no longer symmetric about the y axis and has been shifted to the left of the origin. Thus, as ξ varies, the distribution that passes through the aper-

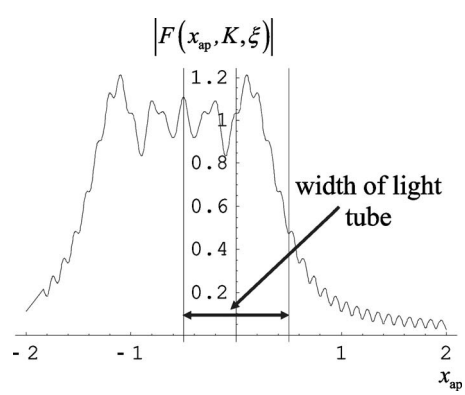

Fig. 3. Magnitude distribution of $F(x_{\mathrm{ap}},K,\xi)$ for $K=15.7$ and $\xi=0.5$.

ture changes, and the system can no longer be considered shift invariant. There are two perpendicular lines inserted in the figure, marking the boundaries of the light tube predicted from a ray optics model (see Fig. 1). Diffraction can act to either spread light outside this light tube or focus the light along the optical axis [10]. The form of the wave field incident on the aperture can thus determine the amount of power that passes through to the image plane. As a result, the power in the image plane, predicted using the LSI and SPM models, is in general not equivalent.

The first term (square brackets) in Eq. (9) is a linear phase term and is identical to the term in Eq. (7). The second term (curly brackets) describes the form of the distribution and has a dependency on the ξ term, which is the normalized displacement of the point source in the object plane. Dividing Eq. (9) by Eq. (7) gives

$$\frac{U_{\mathrm{ap}}(x_{\mathrm{ap}})}{U_{\mathrm{pw}}(x_{\mathrm{ap}})} = F(x_{\mathrm{ap}},K,\xi)\exp(j\Delta\phi') = \mathrm{erfi}[\sqrt{jK}(x_{\mathrm{ap}}+\xi-1)] - \mathrm{erfi}[\sqrt{jK}(x_{\mathrm{ap}}+\xi+1)], \tag{10}$$

where $F(x_{\mathrm{ap}},K,\xi)$ and $\exp(j\Delta\phi')$ represent the magnitude and phase deviations between the LSI and the SPM models, respectively [10,11].

Recently [10] we investigated a similar diffraction problem, examining the deviations between ideal and nonideal converging spherical waves where the nonideal wave is formed using a converging lens of finite extent. We derived a set of curves that pass through the phase and magnitude deviation extrema [10,11]. These curves are a function of the wavelength of light, lens diameter and focal length, the distance from the lens, z_s, and the perpendicular distance from the optical axis x_s. In Eq. (11) we reproduce an equation originally presented in Ref. [10]:

$$x_s = \frac{N\pi z_s}{4}\frac{1}{K}. \tag{11}$$

In Refs. [15,16], propagating collimated and converging beams with the Fresnel transform is discussed. Using the results and insight provided by Ref. [15] in particular, we can extend the applicability of Eq. (11) [10] to the diffraction problem we are considering in this paper. We are concerned with deviations in the distribution at the Fourier (aperture) plane, which is the focal plane of L_1, and so we set $z_s=f_1$ and $x_s=x_{\mathrm{ap}}$. In Fig. 4 we present magnitude deviation plots for Eq. (10) for $5<K<20$ and $-0.4<x_{\mathrm{ap}}<1$ with $\xi=0$.

The curves given by Eq. (11) are overlayed on the figure. Only curves with an even value for the integer parameter N are seen to lie on the magnitude maximum deviations [10,11]. Although only magnitude deviations are shown in Fig. 4, Eq. (11) is also valid for phase deviation extrema [10,11].

B. Deviations in the Image Field Distribution

Assuming that the lens L_2 is infinite, the field distribution in the image plane is given by a scaled Fourier transform:

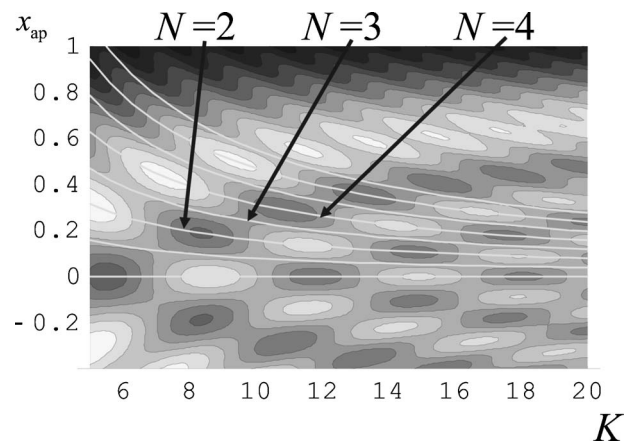

Fig. 4. Magnitude deviations of $F(x_{\mathrm{ap}},K,\xi)$ with $\xi=0$. The deviations range between a minimum of 0.5 and a maximum of 1.2 and are marked with ten contour levels.

$$U_{\mathrm{im}}(x'_{\mathrm{im}}) = \mathcal{F}\{U_{\mathrm{ap}}(x_{\mathrm{ap}})p(x_{\mathrm{ap}})\}(u)\Big|_{u\to x'_{\mathrm{im}}/\lambda f_2}. \tag{12}$$

An analytical solution for Eq. (12) can be found in Ref. [17].

To compare the deviations between LSI and SPM models, we calculate the RMSE of distributions over the range R in the image plane, i.e.,

$$\Omega = \sqrt{\int_{-R+\xi L}^{R+\xi L} |I_{\mathrm{LSI}}(a_N,K) - I_{\mathrm{SPM}}(a_N,K)|^2 \mathrm{d}x_{\mathrm{im}}}, \tag{13}$$

where I_{LSI} and I_{SPM} denote the predicted LSI and SPM intensity distributions, respectively; $a_N=a/L$, where a is the Fourier plane aperture radius; and $R=\lambda/(5a)$. We note that the power contained in the ideal (LSI) PSF over this range, $2R$, is 97.5% of the total power present at the Fourier plane aperture.

In all of the following analysis, $f_2=f_1$, ensuring that the systems have unit magnification. In Fig. 5 we present plots of the intensities in the image plane with $K=15.7$ and $a_N=0.25$ for the three cases in Figs. 5(a)–5(c) with $\xi=0$, $\xi=0.75$, and $\xi=1$, respectively. We refer to the RMSE in each case as Ω^{a}, Ω^{b}, etc., while the powers in the image plane are P^{a}, P^{b}, etc.

In Fig. 5(a) the LSI intensity distribution is also plotted for comparison (dashed curve). We see that both the LSI and the SPM PSFs are symmetric about the y axis and $\Omega^{\mathrm{a}}=0.0039$. In Fig. 5(b), $\xi=0.75$, and there is a noticeable asymmetry in the PSF. In this case $\Omega^{\mathrm{b}}=0.0357$ compared with $\Omega^{\mathrm{a}}=0.0039$. A ray analysis predicts that this point is the vignetting limit (see Section 2). We also note that $P^{\mathrm{b}}=0.045$ is considerably less than P^{a}. Finally, in Fig. 5(c), we present the PSF when $\xi=1$. The shape of the PSF is distorted, with $\Omega^{\mathrm{c}}=0.1491$ and $P^{\mathrm{c}}=0.017$, both of which are significantly worse than in the two previous cases.

In each case of Figs. 5(a)–5(c) the PSF changes, and as ξ increases the corresponding PSF becomes increasingly asymmetric. Clearly this system is no longer shift invariant.

Thus far, to examine the deviations between the LSI and the SPM models, we have used a specific value of K. We now wish to examine how these deviations vary as a function of K. Setting $a_N=0.25$, we plot $\log_{10}(\Omega)$ for 5

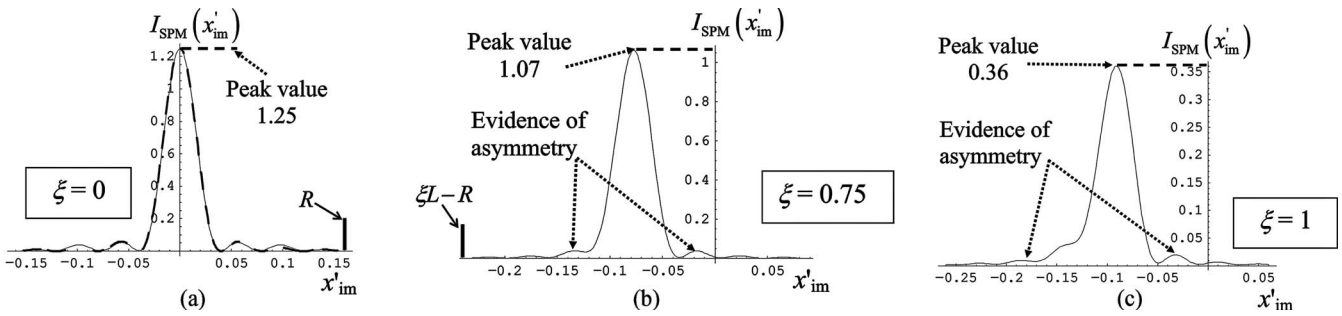

Fig. 5. Intensity of image distribution for $a_N=0.25$, $\Omega^a=0.0039$, and $P^a=0.050$. LSI PSF is also plotted (see dashed curve). (b) Intensity of image distribution at the vignetting limit: $\xi=0.75$, $a_N=0.25$, $\Omega^b=0.0357$, and $P^b=0.045$. (c) Intensity of image distribution for $\xi=1$, $a_N=0.25$, $\Omega^c=0.1491$, and $P^c=0.017$.

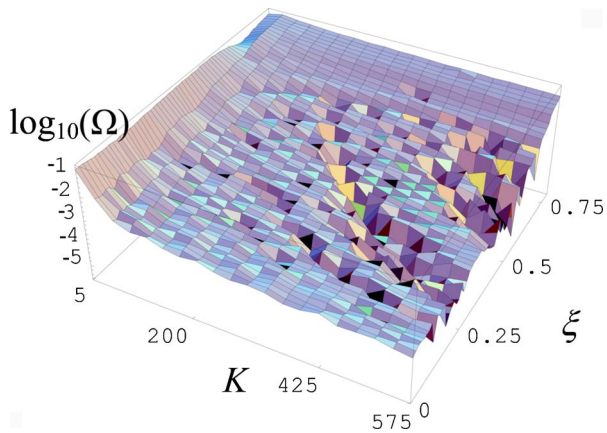

Fig. 6. (Color online) Variation of Ω as a function of K and ξ.

$<K<575$ and $0<\xi<0.775$ in Fig. 6. We draw the reader's attention to two points: (1) as ξ increases, so too does Ω for all values of K, and (2) as K increases, Ω decreases, indicating that the deviations between the two models decrease. In a practical optical system, e.g., $K=590524$ (i.e., $\lambda=532$ nm, $L=10$ cm, $f=10$ cm), $\Omega\sim 1.3\times 10^{-7}$.

C. Effect on the Optical Transfer Function

If an imaging system can be modeled as linear and shift invariant, then its incoherent imaging ability can be conveniently described using the OTF, given by a scaled version of the autocorrelation of the generalized pupil function [3]. The term generalized pupil function is used to indicate that lens aberrations can be included in the pupil function with the result that it may no longer be a real function [3].

In this subsection we incorporate the diffraction effects due to the finite extent of L_1 using Eq. (10) to write a generalized pupil function $p_g(x_{ap})$ as follows:

$$p_g(x_{ap}) = p(x_{ap})F(x_{ap},K,\xi)\exp(j\Delta\phi'). \tag{14}$$

The OTF, $H_{SPM}(\varpi)$, of the SPM optical system is found by calculating the normalized autocorrelation of p_g; see Eq. (15). Using a variable, ϖ, that has been normalized with respect to the aperture size, a, such that $\varpi=x_{ap}/a$, gives

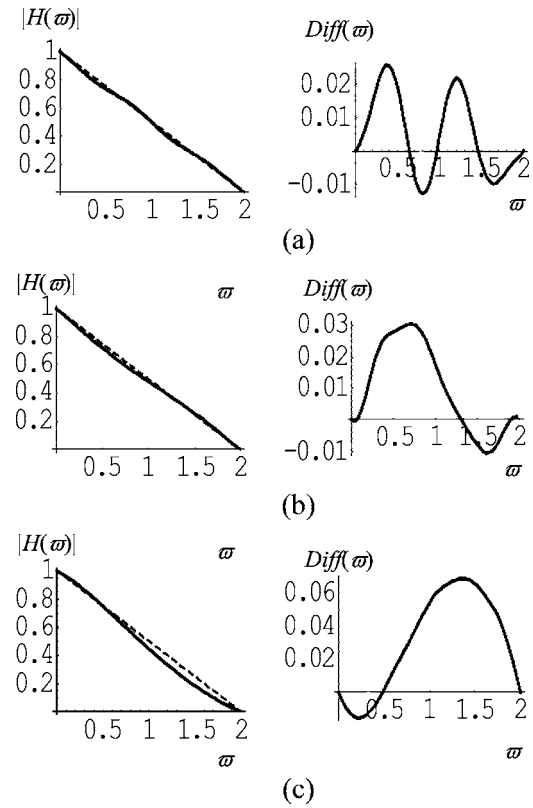

Fig. 7. $|H(\varpi)|$ of LSI (dashed lines) and SPM (solid curves) with $a_N=0.25$ (left column) and $\mathrm{Diff}(\varpi)=|H_{LSI}(\varpi)|-|H_{SPM}(\varpi)|$ (right column). (a) $\xi=0$, (b) $\xi=0.5$, (c) $\xi=0.75$.

$$H_{SPM}(\varpi) = \frac{p_g(\varpi) * p_g(\varpi)}{\int_{-\infty}^{\infty} |h_{SPM}(u)|^2 \mathrm{d}u}, \tag{15}$$

where $h_{SPM}(u)$ is the Fourier transform of $H_{SPM}(\varpi)$ and * denotes correlation.

In the left-hand plots of Figs. 7(a)–7(c), the magnitudes of the LSI and SPM OTFs, $|H(\varpi)|$, are presented for $\xi=0$, 0.5 and 0.75. The LSI OTF, $H_{LSI}(\varpi)$, is calculated by performing the autocorrelation of the aperture function given by Eq. (5) and normalizing with respect to the total power in the aperture opening as outlined in Chap. 6 of Ref. [3]. The SPM OTF, $H_{SPM}(\varpi)$, is given by Eq. (15) and is calculated numerically [14,17]. In order to highlight the devia-

tions between the two models, we also provide plots of the absolute difference between the LSI and SPM OTFs, $\mathrm{Diff}(\varpi)=|H_{\mathrm{LSI}}(\varpi)|-|H_{\mathrm{SPM}}(\varpi)|$, for the three situations, when $\xi=0$, 0.5 and 0.75.

Equation (15) was evaluated for $K=15.7$, $a_N=0.25$, and for [Fig. 7(a)] $\xi=0$, [Fig. 7(b)] $\xi=0.5$, and [Fig. 7(c)] $\xi=0.75$. In Figs. 7(a)–7(c) we present the results using the normalized variable ϖ. The dashed lines represent the LSI case and the solid curves the SPM case. As can be seen, the OTF changes as ξ varies, emphasising again that the imaging operation is not performing space-invariant incoherent imaging. In Fig. 7(a) the magnitude difference is less than in both Figs. 7(b) and 7(c). This is in keeping with the analysis presented in Subsection 3.B. As ξ increases, the difference between the predictions of the LSI and SPM models becomes larger.

D. Imaging of a Semi-Infinite Straight Edge

In this subsection we examine coherent and incoherent imaging of an edge for the LSI and SPM cases. Mathematically we model a 1-D edge using the unit-step function [14,18]

$$\mathrm{step}(x)=\begin{cases}1, & x\geq 0\\ 0, & x<0\end{cases}. \tag{16}$$

When comparing the coherent and incoherent cases we will examine the behavior for two situations, an on-axis and an off-axis centered edge. Mathematically we model these cases using step (x_{obj}) and step $(x_{\mathrm{obj}}-\xi)$, where ξ is the location, off axis in the object plane, where the edge occurs.

Examining Eq. (16), we can see that the edge, as defined, extends to +/−infinity in the object plane. We know, however, from Section 3 that a ray-based analysis predicts that the image of such an object will begin to taper off to zero as we pass the vignetting limit (see Fig. 2). In other words, even with the LSI model we do not expect our system to be capable of imaging all the rays from an infinite object plane to an infinite image plane. Thus when simulating the LSI case we include the effects of vignetting as described in Section 2.

To make our results as general as possible, in the following figures the image plane axis, x'_{im} is normalized with respect to the diameter of L_1 and $x_{\mathrm{im}}=x'_{\mathrm{im}}/L$. This time we choose a larger value for K, $K=157$, and set $a_N=0.25$. When this diffraction problem was considered by Considine [18] and Goodman [3], the vignetting effects in the LSI case were neglected and the intensities in the image plane were normalized so that they approached unity as x_{im} approached infinity (see Fig. 7.20 in Ref. [3]). We normalize the LSI and SPM intensities in the image plane in the same manner and refer to them as $I'_{\mathrm{LSI}}(x_{\mathrm{im}})$ and $I'_{\mathrm{SPM}}(x_{\mathrm{im}})$, respectively.

1. Coherent Imaging

We note one feature that is common to the distributions predicted by the LSI and SPM models that can be important in estimating the widths of lines in integrated circuit masks [3], namely, the point at which each distribution crosses the edge [see Fig. 8(a)]. We refer to this point as $\mathrm{CR}^C_{\mathrm{LSI}}$ or $\mathrm{CR}^C_{\mathrm{SPM}}$, where the superscript C denotes coherent imaging. In Fig. 8(a) we present the results for an on-axis edge. Note that the values of both the LSI and the SPM field intensities as they cross the edge are $\mathrm{CR}^C_{\mathrm{LSI}}=\mathrm{CR}^C_{\mathrm{SPM}}=0.25$.

The ringing observed in the coherent images is reminiscent of Gibb's phenomenon that occurs at discontinuities when the Fourier series expansion is used. This effect is strongest when discontinuities in the object are imaged, and thus strong oscillations are evident at the location of the discontinuity $x_{\mathrm{im}}=0$. If we could neglect the vignetting effects in the imaging system, these oscillations would decay asymptotically toward unity [18]. However, when vignetting effects are included in the LSI model there is a corner at the vignetting limit $x_{\mathrm{im}}=0.75$, the derivative of which is discontinuous. This causes the oscillations to once again increase in amplitude as $x_{\mathrm{im}}>0.5$. Since the SPM model images only a finite region of the object plane, due to the finite extent of L_1, the vignetting effects are already included in this model. We do note, however, that the frequency of the oscillations around the edge or discontinuity for the SPM case appears to be higher than for the LSI case, with the result that at $x_{\mathrm{im}}=0.8$ the LSI and SPM distributions are almost exactly out of phase.

In Fig. 8(b) we present the LSI and SPM distributions for the case of an off-axis edge, and once again $\mathrm{CR}^C_{\mathrm{LSI}}=\mathrm{CR}^C_{\mathrm{SPM}}=0.25$. There are strong oscillations around the discontinuity and corner points associated with the edge and the vignetting limit, respectively.

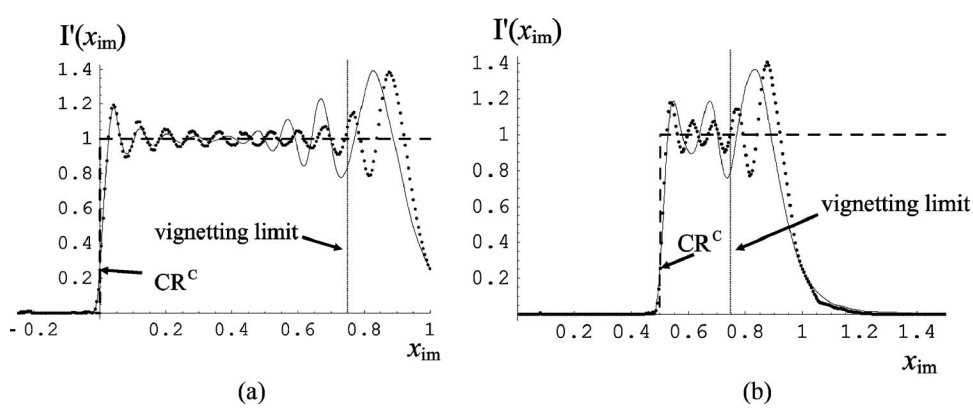

Fig. 8. LSI (solid curve) and SPM (dots) coherent distributions in the image plane for a 1-D step centered at $\xi=0$, $K=157$, and $a_N=0.25$. (b) LSI (solid curve) and SPM (dots) distributions for a 1-D step centered at $\xi=0.5$.

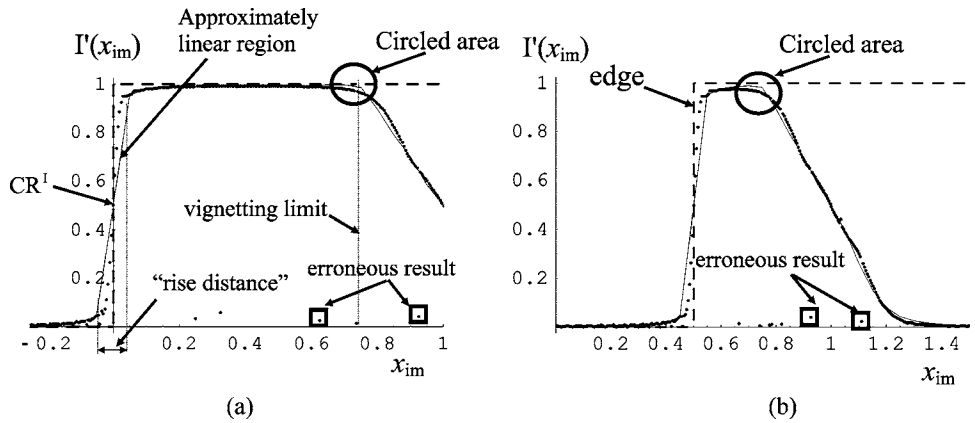

Fig. 9. LSI (solid curve) and SPM (dots) incoherent distributions in the image plane for a 1-D step centered at $\xi=0$, $K=157$, and $a_N=0.25$. (b) LSI (solid curve) and SPM (dots) distributions for a 1-D step centered at $\xi=0.5$.

2. Incoherent Imaging

The incoherent response of the system to the semi-infinite edge is displayed in Fig. 9(a) with $\mathrm{CR}^I_{\mathrm{LSI}}=\mathrm{CR}^I_{\mathrm{SPM}}=0.5$. In Fig. 9(a) we note that as the LSI (solid curve) and SPM (dots) distributions rise from zero to unity there is a region where the slope in both cases is approximately linear but different, with the SPM rising more rapidly. In control engineering there is a common performance metric for describing the responses of systems to a sudden input or load (usually a unit step), which is termed the rise time. It is defined as the time taken for the system to go from 10% to 90% of its new steady-state value [19]. We now use a similar rise distance metric and illustrate what we mean graphically in Fig. 9(a) for the LSI case.

From inspection of Fig. 9(a) it would appear that the rise distance in the SPM case is less than in the LSI case, indicating an improved response. Also, we note that the vignetting limit occurs at $x'_{\mathrm{im}}=0.75$, and in this region [the circled area in Fig. 9(a)] the SPM response appears to drop off more quickly than in the LSI case. This we attribute mainly to the degradation in the PSF in the circled region due to diffraction effects from the aperture at L_1; see Figs. 5(a)–5(c) and Figs. 7(a)–7(c).

We now consider the response of the imaging system for an off-set or off-axis edge, i.e., unit step $(x_{\mathrm{obj}}-\xi)$. In Fig. 9(b) we present the results with, once again, $\mathrm{CR}^I_{\mathrm{LSI}}=\mathrm{CR}^I_{\mathrm{SPM}}=0.5$, and the rise distance for the SPM is less than that for the LSI case. We again draw attention to the degradation of the SPM response near the vignetting limit point (see circled region).

We note that the results presented in Figs. 9(a) and 9(b) require the numerical calculation of integrals that exhibit unstable convergence. This sometimes produces erroneous results, some of which for completeness are highlighted with gray boxes in Figs. 9(a) and 9(b).

E. Effect of a Finite-Size Lens L_2 on the Distribution in the Image Plane

Earlier in this section we made the assumption that L_2 was effectively infinite in extent. This assumption allowed us to derive an analytical solution for the distribution in the image plane arising from a point source in the object plane. In this subsection we wish to examine specifically how the finite extent of the second lens affects the imaging system performance. Assuming that the input to the imaging system is a point source located on axis in the object plane, we examine how Ω varies as a function of the radius of L_2, denoted Λ. We again choose $K=15.7$, $L=10$ cm, and $a_N=0.25$. We are not aware of an analytical solution for this case, and so the following Ω values were calculated numerically [20]. In Fig. 10 we present the results. The dashed line indicates the size of Ω when Λ is assumed infinite and is plotted for comparative purposes. Ω decreases rapidly (solid curve) as Λ approaches L, and, indeed, once $\Lambda>L$, the solid curve and dashed line quickly converge, indicating that effects of diffraction from the second lens can effectively be neglected.

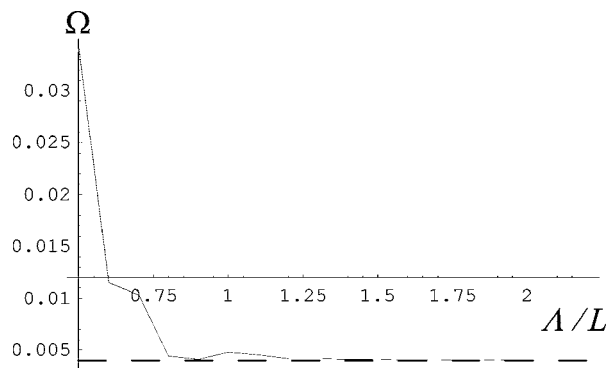

Fig. 10. Variation of Ω with $K=15.7$, $L=10$ cm, and $a_N=0.25$ as a function of Λ (solid curve). Dashed line indicates corresponding Ω when $\Lambda\to\infty$.

In Fig. 11 we examine in more detail the effect the second lens aperture has on the final image plane intensity distribution, $I^{\Lambda}_{\mathrm{SPM}}(x'_{\mathrm{im}})$. In the top graph we set $\Lambda=L$ and plot $0<I^{\Lambda}_{\mathrm{SPM}}(x'_{\mathrm{im}})<0.2$ over the range $0<x'_{\mathrm{im}}<R$. The LSI PSF is plotted as a dashed curve, again for comparative purposes. It is expected that the second lens aperture will remove some of the incident wave field distribution, affecting the final image plane distribution. The effect can be seen clearly in the top graph of Fig. 11 [$I^{\Lambda}_{\mathrm{SPM}}(x'_{\mathrm{im}})$ is plotted as a solid curve]. For example, the second sidelobe of $I^{\Lambda}_{\mathrm{SPM}}(x'_{\mathrm{im}})$ is distorted and slightly oscillatory when compared with the LSI PSF. In the bottom graph of Fig. 11, we plot the same distribution, this time with $\Lambda=1.5L$. In this instance, less of the distribution incident upon L_2 is

removed by the aperture. The result is that the second sidelobe associated with the $I^{\Lambda}_{\mathrm{SPM}}(x'_{\mathrm{im}})$ distribution becomes smooth and in fact larger than the corresponding LSI sidelobe, consistent with the results presented in Figs. 5(a) and 10.

4. CONCLUSION

In Chap. 6 of Goodman's *Introduction to Fourier Optics* [3], an imaging system consisting of several optical elements is modeled as a linear shift-invariant (LSI) system. Diffraction effects in the imaging process are attributed to a single limiting aperture somewhere in the system with the assumption that all other apertures are effectively infinite in extent. Taking the case of the 4-*f* imaging system, we examined this approximation in detail by comparing the response of the LSI model to what we term the superposition model (SPM), including diffraction effects due to the finite extent of a lens, L_1. As was shown in Subsection 3.A, the LSI model indicates that the limiting aperture in the Fourier plane is illuminated by a perfect plane wave. However, the SPM model indicates that the aperture is in fact illuminated by a more complex wave field. As we saw in Subsection 3.E, once $\Lambda > L$, the effect of diffraction from the second lens, L_2, has a much less significant impact on the final output distribution in the image plane than does L_1. Thus it is the differences between the LSI and the SPM representations of the system that effectively represent the fundamental paraxial diffraction limits. We proceed to analyze these differences for the remainder of Section 3.

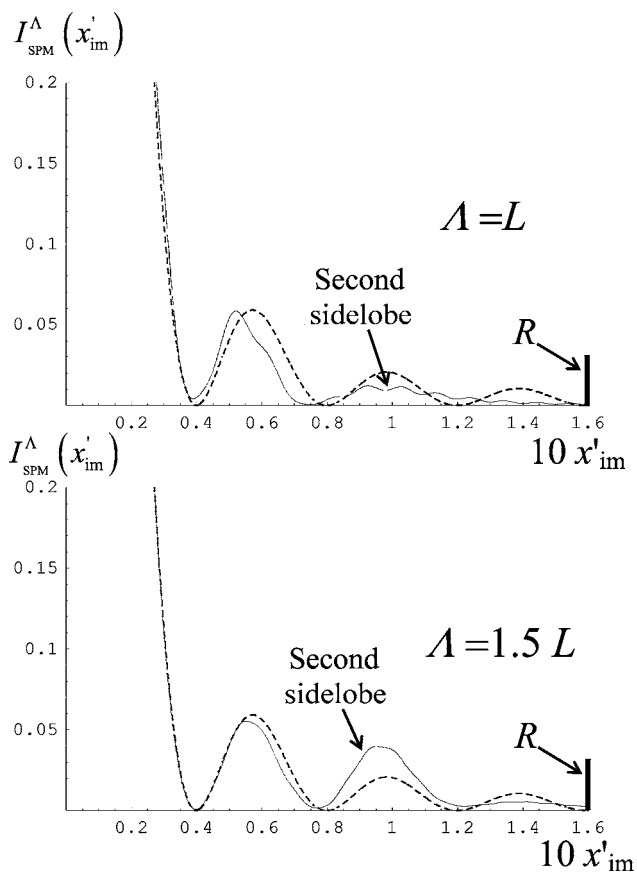

Fig. 11. $I^{\Lambda}_{\mathrm{SPM}}(x'_{\mathrm{im}})$ refers to the distribution in the image plane when diffraction from both L_1 and L_2 is considered. LSI PSF is also plotted (see dashed curves in plots). Top, $\Lambda = L$; bottom, $\Lambda = 1.5L$.

In Subsection 3.B the response of the SPM model to several point sources in the object plane located at different off-axis distances, $\xi = 0$, $\xi = 0.75$, etc., are presented. It is clear from examining Figs. 5(a)–5(c) that the system does not perform space-invariant imaging.

In Subsection 3.C we consider the incoherent performance of the system by examining a modified version of the optical transfer function (OTF). This modified OTF is dependent on spatial position in the object plane, again demonstrating that the 4-*f* imaging system does not perform space-invariant imaging.

Finally, in Subsection 3.D we compare the imaging of an edge (unit-step) function using the LSI and SPM models. Again, there are differences between the LSI and the SPM predictions; however, significantly, the cross-over point, CR, (see Subsection 3.D) for both models occurs at $\xi = 0.25$ (coherent case) and $\xi = 0.5$ (incoherent case).

We conclude that (i) when diffraction effects from lens apertures are included in the analysis of a 4-*f* imaging system, the system no longer performs shift-invariant imaging; (ii) once the extent of L_2 is greater than that of L_1 (in a unit magnification system), the resultant PSF (apart from some distortion of the second sidelobe; see Fig. 11) remains largely unaffected by changes in the diameter of L_2; and (iii) the deviations between the LSI and the SPM models dramatically reduce in size as K approaches values used in practical optical systems, e.g., when $K \sim 6 \times 10^5$, $\Omega \sim 1.3 \times 10^{-7}$. In this case, as expected, an LSI analysis is sufficient. It is, however, of fundamental importance that the ultimate performance limitations of an imaging system in the paraxial regime be fully understood and quantified.

While the manuscript was under review, it came to the author's attention that a paper examining the effect of diffraction from multiple apertures in an optical system on the power transmitted to the output plane has previously been published and may serve as an interesting companion to the work presented here [21].

ACKNOWLEDGMENTS

We acknowledge the support of the Enterprise Ireland and Science Foundation of Ireland through the Research Innovation Fund, the Basic Research Programme, and the Research Frontiers Programme. We also acknowledge the support of the Irish Research Council for Science, Engineering, and Technology.

REFERENCES

1. E. L. O'Neill, *Introduction to Statistical Optics* (Addison-Wesley, 1962).
2. R. N. Bracewell, *The Fourier Transform and Its Applications*, Int. ed. (McGraw-Hill, 1986).
3. J. W. Goodman, *Introduction to Fourier Optics*, 3rd ed. (Roberts, 2005).
4. E. Hecht, *Optics*, 2nd ed. (Addison-Wesley, 1989).
5. W. T. Rhodes, *Lecture Series: Fourier Optics and*

Holography (Imaging Technology Center, Florida Atlantic University, 2006).
6. R. W. Dichtburn, *Light* (Dover, 1965).
7. M. Gu, *Advanced Optical Imaging Theory*, 1st ed. (Springer-Verlag, 2000).
8. T. Wilson and C. Sheppard, *Theory and Practice of Scanning Optical Microscopy* (Academic, 1984).
9. J. T. Sheridan and C. J. R. Sheppard, "Modelling of images of square-wave gratings and isolated edges using rigorous diffraction theory," Opt. Commun. **105**, 367–378 (1994).
10. D. P. Kelly, J. T. Sheridan, and W. T. Rhodes, "Finite-aperture effects for Fourier transform systems with convergent illumination. Part I: 2-D system analysis," Opt. Commun. **263**, 171–179 (2006).
11. D. P. Kelly, J. T. Sheridan, and W. T. Rhodes, "Finite-aperture effects for Fourier transform systems with convergent illumination. Part II: 3-D system analysis," Opt. Commun. **263**, 180–188 (2006).
12. M. Abramowitz and I. A. Stegun, *Handbook of Mathematical Functions* (Dover, 1970).
13. I. S. Gradshteyn and I. M. Ryzhik, *Table of Integrals, Series, and Products* (Academic, 1980).
14. S. Wolf, *The Mathematica Book*, 4th ed. (Cambridge U. Press, 1999).
15. G. W. Forbes, "Scaling properties in the diffraction of focused waves and an application to scanning beams," Am. J. Phys. **62**, 434–443 (1994).
16. G. W. Forbes, "Validity of the Fresnel approximation in the diffraction of collimated beams," J. Opt. Soc. Am. A **13**, 1816–1826 (1996).
17. D. P. Kelly, "Linear quadratic phase systems and their application to speckle photography based metrology systems," Ph.D. dissertation (National University College Dublin, Ireland, 2006).
18. P. S. Considine, "Effects of coherence on imaging systems," J. Opt. Soc. Am. **20**, 661–667 (1966).
19. K. Dutton, S. Thompson, and B. Barraclough, *The Art of Control Engineering* (Addison-Wesley, 1997).
20. D. P. Kelly, B. M. Hennelly, W. T. Rhodes, and J. T. Sheridan, "Analytical and numerical analysis of linear optical systems," Opt. Eng. **45**, 088201 (2006).
21. E. L. Shirley, "Intuitive diffraction model for multistaged optical systems," Appl. Opt. **43**, 735–743 (2004).